NUMERICAL FLOWFIELD VISUALIZATION OVER HEAT SHIELD OF SATELLITE LAUNCH VEHICLE AT MACH 0.8 - 3.0

R. C. Mehta
Professor
Department of Aeronautical Engineering
NI University, Kumaracoil, India
Formally Senior Fellow
School of Mechanical and Aerospace Engineering
Nanyang Technological University
Singapore-639 798
Email : atulm@md4.vsnl.net.in

Abstract

The paper presents a numerical flowfield visualization over a typical payload shroud of a satellite launch vehicle at Mach number range of 0.80 -3.0 and Reynolds number range of 33 x 10^6 - 46 x 10^6/m. The numerical simulation over the bulbous heat shield is carried out by solving time-dependent compressible axisymmetric turbulent Reynolds-averaged Navier-Stokes equations. The closure of these equations is obtained employing the Baldwin-Lomax turbulence model. A three-stage Runge-Kutta time-stepping scheme has been used in conjunction with finite-volume discretization of the computational domain. The flowfield features over the bulbous heat shield have been analyzed from the velocity vector and the density contour plots. Flow separation on the payload shroud due to the normal shock wave is observed at Mach number 0.80 and 0.90. The normal shock movement on the heat shield is simulated for various transonic Mach number. A recirculation zone of flowfield is formed in the boat-tail region of the heat shield. The vorticity formation ahead of the heat shield moves close to the heat shield with the increasing transonic Mach number, which is observed in the density contours plots of the flowfield. Shock stand-off distance at the supersonic speed is calculated and compared with asymptotic formula of Frank and Zierep. They are found in good agreement.

Introduction

A bulbous payload shroud is generally selected to accommodate an increase payload volume of the satellite in a launch vehicle. The heat shield in any launch vehicle is needed to protect the satellite from aerodynamic loading, heating, aero-acoustic vibration, and other environmental conditions during the ascent phase of the flight and to provide aerodynamic forward surface. The estimation of flowfield characteristics around such a heat shield configuration is of great aerodynamic important, as well as research interest. For the ascent flight, during the transonic speed range, their study is particular important because of such resulting phenomena as normal shock movements, frequently coupled with substantial freestream dynamic pressure. These parameters directly depend on the intensity of the vorticity components of the turbulence, the strength of the shock, and the mechanism of their interaction, all of which are implicitly linked to the specific configuration of the heat shield. The numerical flow simulation over a bulbous payload shroud at transonic Mach number range is very useful to decide the geometrical configuration for minimum buffeting load and minimum aerodynamic drag requirement. The terminal shock wave of sufficient strength intersecting with boundary layer can cause flow separation and flow field may become unstable as observed in the high speed cinematography [1]. Therefore, it is desirable to determine the location of the normal shock on the heat shield and the strength of the normal shock as a function of transonic Mach numbers. The strength of the normal shock wave and the mechanism of

Paper Code : V63 N3/746-2011. Manuscript received on 07 Mar 2011. Reviewed and accepted as a Full Length Contributed Paper on 21 July 2011

their interaction are related to the specific configuration of the heat shield satellite launch vehicle. The features of the transonic flow field can be delineated through the wind-tunnel data such as schlieren photographs and oil flow patterns. It is characterized by a normal or terminal shock, supersonic pocket on the cylindrical region of the heat shield, shock wave/turbulent boundary layer interaction, and a separated bubble may be caused by the shock wave/turbulent boundary layer on the cylindrical section of the heat shield. The main features of transonic flow field around a bulbous heat shield are illustrated in Fig.1(a). In the boat-tail region, a local separation results, due to sharp discontinuity in the longitudinal of the payload shroud. The regions of flow separation impose additional complexity to aerodynamic and structural design aspects [2-5]. The complex flow field at the transonic speeds is also observed during the experimental investigation of the bulbous heat shield. Experimental investigations were limited to the measurement of surface pressure distribution, oil flow patterns, and schlieren picture [6]. Fig.1(b) delineates the schematic sketch of the supersonic flow over the heat shield. A bow shock wave is formed ahead of the heat shield and the bow shock wave stand-off distance is measured from the stagnation point of the heat shield. The flow decelerates through the bow shock wave depending upon the supersonic Mach number. A sonic line is located at the junction of the spherical blunt cone junction. The shock stand-off distance is function of freestream Mach number and radius of the blunted cone of the heat shield. The bow shock wave in front of the heat shield causes high surface pressure and result the development of high aerodynamic drag during the ascent period of the flight. The aerodynamic drag at the supersonic Mach number is important input parameters for designing the payload capability of the launch vehicle, which needs a complete analysis of the flow field around the heat shield from transonic to supersonic speeds.

Flowfield over three-different type of heat shield configurations have been computed numerically by Deese et. al [7] using a multi-stage Runge-Kutta time-stepping method. After comparing results with the wind-tunnel data, it was found that the Baldwin-Lomax turbulence model [8] is more accurate than the two-equation turbulence model. Purohit [9] has analyzed a typical bulbous heat shield using MacCormack's explicit scheme in conjunction with an algebraic turbulence model for a freestream Mach number 0.8. Numerical simulation of flow field over a bulbous heat shield at transonic and supersonic speed [10] is carried out by solving the time-dependent compressible axisymmetric turbulent Reynolds averaged Navier-Stokes equations in order to compare the numerical analysis with the wind-tunnel results. Owens [11] has carried out experimental investigation to determine the aerodynamic characteristics and effects of bluntness of spherically blunted cones at Mach numbers from 0.5 to 5.0. For the various heat shield configurations of satellite launch vehicle, the available experimental data are not sufficient to determine the movement of the normal shock; the shock wave induced separated flow on the fore-body of the cylinder, the flow separation zone due to boat-tail, and the shock stand-off distance on blunted cone at the supersonic speeds. Thus, a complete analysis of the flow field around the payload shroud is required to understand the flow field characteristics at transonic to supersonic Mach number ranges.

The present study employs a Computational Fluid Dynamics approach to analyze a complex fluid dynamics problem of the payload shroud of the satellite launch vehicle in the Mach number range of 0.80 - 3.0 and Reynolds number range of 33×10^6 - 46×10^6/m. The time-dependent compressible turbulent axisymmetric Reynolds-averaged Navier-Stokes equations are solved using a finite volume discretization of computational domain in conjunction with a three-stage Runge-Kutta time-stepping scheme. The main purpose of the present paper is to generate the flowfield over a typical heat shield of a launch vehicle at transonic to supersonic speeds. The numerically generated flowfield visualization and analysis will help to understand complex transonic as well as supersonic flowfield features on the heat shield. Thus, the selection of the bulbous payload shroud can be done employing numerical simulation before testing the model in the wind-tunnel. The flowfield characteristics are analyzed with the help of vector and density contour plots.

Flow Solver

Conservation Equations and Turbulence Modeling

The time-dependent, compressible, turbulent, axisymmetric Reynolds-averaged Navier-Stokes (RANS) equations are written in integral form [10]. The temperature is related to pressure and density by perfect gas equation of state. The ratio of the specific heats γ is assumed constant and is equal to 1.4. The coefficient of molecular viscosity is calculated according to Sutherland's law. The closure of the system of equations is achieved by introducing algebraic turbulence model of the Baldwin-Lomax [8].

Spatial Discretization

The Reynolds-averaged Navier-Stokes equations are written in the integral form [10] over the computational domain surrounding the heat shield. The numerical method uses a finite volume discretization scheme in space without any intermediate mapping. The spatial and temporal terms in the integral form of the differential equation are decoupled using the method of lines. It has a major advantage of direct discretization of the fluid dynamics equations in the physical domain. The spatial computational domain of over the heat shield is divided into a finite number of non-overlapping structured quadrilateral cells. The conservative variables of each cell are calculated from their average values at the cell centre. The flow variables are stored in the centre of the cell. On each cell face the convective and diffusive flux vectors are computed on each side of the quadrilateral grid [12]. The numerical procedure now reduces to central differencing on a quadrilateral and smooth grid. The entire spatial discretization scheme reduces to a central-difference scheme and is second-order accurate in space. In the viscous flux calculations, the dissipative properties are present due to diffusive terms.

Temporal Discretization

Temporal integration is carried out by the three-stage time-stepping [13], based on the Runge-Kutta scheme. The numerical method needs an additional artificial dissipation term to prevent odd-even decoupling and to control numerical oscillations in the vicinity of severe pressure gradients. Away from the shear layer region, the physical diffusion is generally not adequate to prevent the odd-even point decoupling of the centered numerical scheme. Thus, to maintain numerical stability and to prevent numerical oscillations in the vicinity of shocks or stagnation points, artificial terms [13] are included as blend of a Laplacian and biharmonic operator in a manner analogous to the second- and fourth-differences. The term involving the second-order difference is switched on to damp numerical oscillations near shock waves and the term the fourth-order dissipation is added everywhere in the flow domain where the solution is smooth but is switched off in the region of shock waves. The scheme is stable for a Courant number less than or equal to 2. Local time steps are used to accelerate convergence to a steady-state solution by setting the time step at each point to the maximum value allowed by the local Courant-Friedrichs-Lewy (CFL) condition. The above numerical scheme is described in detail in Ref. [14].

Boundary Conditions

At the surface of the payload shroud, no slip condition is considered together with an adiabatic wall condition. At the inflow, all of the flow variables are taken at the freestream condition. A symmetry condition is applied on the centre line ahead of the heat shield.

For the transonic case, non-reflecting far-field boundary conditions are applied at the outer boundary of the computational cell.

For the supersonic flow, all of the flow variables are extrapolated at the out flow from the vector of conserved variables. They are linearly extrapolated at the outer boundary of the computational domain from the conserved variables.

Heat Shield Geometry

The maximum payload shroud diameter D of the model is 0.04 m and the booster diameter d is 0.035m. The spherical cap radius R is 0.00875 m. The symbols D, d, and R are depicted in Fig.1. The boat tail angle is 15 deg measured clock-wise from the axis with reference to the oncoming flow direction. For the blunt-nosed cone, the inclination at the forebody junction is 20 deg and the total length of the shroud from the stagnation point to the boat tail is 0.083 m.

Computational Grid

The numerical simulation requires the proper grid arrangement in the computational domain. The structured grid generation and the mono block are suitable to accommodate the bulbous heat shield. The following procedure is used to generate grid in the computational region of the bulbous heat shield. The computational domain is divided into number of non-overlapping zone. The mesh points are generated in each zone using finite element method [15] in conjunction with the homotopy scheme [16]. The payload fairing is defined by a number of grid points in the cylindrical coordinate system. Using these surface points as the reference nodes, the normal coordinate is then described by the exponentially stretched [17] grid points extending outwards up to an outer computational boundary. Grid independence tests [10, 14] were carried out, taking into consideration the effect of the computational domain, the stretching factor to control the grid intensity near the wall, and the number of grid points in the axial and normal directions. The outer boundary of the computational domain is varied from 5 to 8.0 times the cylinder

diameter D and the grid-stretching factor in the radial direction is varied from 1.5 to 5. At transonic freestream Mach number, the computational domain of dependence is unbounded, and the implementation of boundary and initial conditions becomes important factor for the selection of the computational region. The known physically acceptable far-field boundary conditions usually limit the flow variables to asymptotic values at large distances from the payload shroud. For the supersonic speeds, the computational domain is kept 3 to 5 times the maximum diameter of the heat shield. The present numerical analysis is carried out on 132 x 62 grid points. For the supersonic speeds, the grid arrangement is described in detail in Ref.[14]. The grid stretching factor is selected 5. The finer mesh near the heat shield surface helps to resolve the viscous effects. The coarse mesh helps in reducing the computer time. The convergence criterion less than the 10^{-5} is based on the difference in the density values at any grid point between two successive iterations. The minimum spacing for the fine mesh is dependent upon the Reynolds number. The finer mesh near the wall helps to resolve the viscous effects. The coarse-mesh helps reducing the computer time. A close-up view of the computational grid over the heat shield is shown in Fig.2. The present grid uses quadrilateral cells in two-dimensional in the computational array as seen in the figure. The quadrilateral cells are very efficient at filling space.

Results and Discussion

The flowfield features around the payload shroud are computed for Mach number range of 0.80 - 3.0 and Reynolds number range of 33×10^6 - 46×10^6/m employing the above described flow solver.

Transonic Flowfield Characteristics

The general flowfield along the complete payload shroud is shown in Fig.3 for freestream Mach number. The figure depicts a close-up view of the velocity vector plots for $M_\infty = 0.80$ and 0.85. The strongly attached flow near the cone-cylinder junction and an expansion due to typical shroud geometry makes way to a flow separation following a normal shock of the supersonic pocket. The separation and reattachment points are marked in the figure as s and r, respectively. The flow separation on the payload shroud is caused by the normal shock wave. The flow separation is confirmed to a short distance, and the flow is reattached at x/D = 1.542 and 1.695 for $M_\infty = 0.80$ and 0.85, respectively. The symbols S and R denote the flow separation due to boat-tail of the payload shroud. The velocity vector and the density contour plots reveals that a shear layer is formed which accommodate the recirculating flow for the transonic speeds. The downstream boundary layer is found to be thick, which is nearly the boat-tail height. It is worth to mention here that the main purpose to introduce the boat-tail is to increase payload volume of a satellite launch vehicle. Fig.4 depicts an enlarge view of the velocity vector plots in the boat tail region of the bulbous heat shield at $M_\infty = 0.95$. It can be observed from the vector plots that the flow separated and enclosing vortex.

Figure 5 depicts the density contour plots for various freestream transonic Mach number. It can be observed from the figures that all of the essential flow field features of the transonic flow, such as supersonic pocket, normal shock, and expansion and compression regions, are very well captured. The density contour plots reveal that the supersonic pocket increases with increasing freestream Mach number. The normal shock wave moves downstream with the increasing transonic speeds. The normal shock wave just reaches the end of the forebody cylinder at $M_\infty = 0.95$. The density contour plots reveal that the supersonic pocket increases with increasing freestream Mach number, and as a result, the terminal shock moves downstream with increasing freestream Mach number. It is important to note here that the formation of the vorticity ahead of the stagnation region of the heat shield. It moves toward the stagnation region with the increasing the transonic Mach number. This flow field feature in the density contour plots is very interesting flow behavior. The shock location obtained from the present numerical results is compared in Ref. [10] and are found in good agreement.

The boundary layer on the cylinder is unable to accommodate steep pressure gradient of the strong terminal shock at $M_\infty = 0.80$ and 0.85. It separates the boundary layer and forming the separation bubble as seen in the vector plots and in the density contour plots. This flow separation is visualized as the shock wave/boundary layer interaction. The shock separated flow information is useful to design the acoustic blanket inside the heat shield to protect the satellite from aero-acoustic vibration. The flow separation in the boat tail region is occurred due to change of geometry of the heat shield. This flow separation is attributed to the bulbous shape of the heat shield. It is having low level pressure fluctuations. The geometrically induced flow separation is observed at freestream Mach number range of 0.8 - 3.0. The flow separation depends on the geometrical parameters of the heat shield and freestream Mach number.

Supersonic Flowfield Characteristics

The close up view of the velocity vector plot for freestream Mach number 1.60 is depicted in Fig.6. In the boat-tail region, a local flow separation results, due to sharp discontinuity in the longitudinal curvature. It can be seen from the figure formation of bow shock wave over the spherical cap region of the payload shroud. The flow field features for the supersonic speeds, the flow turns downstream direction of the boat-tail through an expansion fan resulting shear layer that separates the supersonic flow above the subsonic recirculating region below it. The pressure in the recirculating region is generally uniform and below that of the freestream pressure. As the shear layer impinges on the downstream wall, the flow turns back towards the freestream direction and a recompression shock wave is typically formed.

The density contour plots of Fig.7 show the supersonic flowfield features. Formation of the bow shock wave ahead of the spherical cap of the payload shroud, and a system of weak oblique shock waves downstream of the shoulder of the heat shield which shows an over expansion of the flow. As the freestream supersonic Mach number increases the bow shock wave moves close to the spherical cap of the payload shroud. The density contour plots depict that all the essential flow field features of the supersonic Mach number as delineated in Fig.1(b). It is important to note that all the flowfield features are well captured in the present numerical simulation. The flow turns in the downstream of the boat tail through an expansion fan with a resulting shear layer which separates the supersonic flow above the subsonic recirculating flow below it. As the shear layer impinges on the downstream, the flow turns back toward the freestream direction and a recompression shock wave is generated.

The numerically simulated flow field visualization as depicted in Figs. 5 and 7 can be considered as the Computational Fluid Dynamics generated Schlieren pictures at various freestream Mach numbers.

Bow Shock Wave Stand-off Distance

Figure 8 depicts enlarged view of the velocity vector plots in the vicinity of the sphere-cone region of the heat shield at different values of the supersonic Mach numbers. The bow shock wave distinctly captured, and moves toward the blunted cone region with the increasing freestream Mach number as can also seen in the above density contour plots. The bow shock wave is followed by a subsonic region near the stagnation region as illustrated in Fig.1(b). The bow shock standoff distance is calculated using the following asymptotic formula of Frank and Zierep [18] as

$$\frac{\Delta}{R} = \frac{2(b)^{2/3}}{\left[\dfrac{(M_\infty^2 - 1)}{(\gamma + 1)\, M_\infty^2}\right]^{2/3}} - 1$$

where the value of b is taken as 0.14 [18]. The bow shock wave standoff distance Δ/R versus Mach number is depicted in Fig.9. It can be seen from the figure that the comparison of the present numerical results is in agreement with the asymptotic formula of Frank and Zierep [19].

Surface Pressure Variations

The surface pressure coefficient $\left[C_p = \{(p/p_\infty) - 1\}/(0.5\,\gamma\, M_\infty^2)\right]$ versus non-dimensional length x/D of the heat shield for transonic Mach number and supersonic Mach number is shown in Fig.10(a) and (b), respectively, where the subscript ∞ represents the freestream conditions. The experimental values of the pressure coefficients compare well with the computed results along the length of the payload shroud. Near the stagnation point on the spherical cap, a steep fall in the pressure coefficient was found, which is partially recovered along the cone. The experimental values agree with this trend from the station x/D onward, where the first pressure measurement was made. On the fore body cylinder, the pressure distribution pattern also confirms the movement of the terminal shock, as observed in the density contour plots and depicted in Fig. 5(i). In the boat tail region, the expansion and compressions are comparatively mild. In the case of the transonic Mach number range, the computed results compare well with the experimental data along the entire length of the heat shield except at the cone-cylinder junction, where the maximum expansion of the flow occurs. In the vicinity of the stagnation point and on the spherical region of the heat shield, a sharp fall in the pressure coefficient was observed, which is partially recovered along the conical section of the payload shroud. The experimental data agree with this trend from the location x/D = 0.22 onward, where the first pressure measurement was made. On the fore-body cylinder, the pressure distribution pattern also confirms the movement of the terminal shock wave, as observed in the density

contour plots. In the boat-tail region, the expansion and compression are comparatively mild. The surface pressure coefficient along the heat shield for supersonic Mach number is in good agreement with the experimental data. Detailed comparison of pressure variations are shown in Ref.[10]. It is found that the expansion at the cone fore-body and the boat-tail region reduces with increasing supersonic speeds. For the complete heat shield surface, the expansion at the cone fore-body and the boat-tail region reduces with the increasing freestream supersonic Mach number.

Conclusions

A numerical analysis of axisymmetric turbulent viscous flow over a payload shroud is carried out using a finite volume discretization in conjunction with three-stage Runge-Kutta time-stepping scheme at Mach number range of 0.80 - 3.0 and Reynolds number range of 33×10^6 - 46×10^6/m. The flow field visualization of the terminal shock wave and the separated region helps to systematic understanding of flow structure under various transonic Mach numbers range. The normal shock wave moves downstream with increasing freestream Mach number. An interesting flow field feature is observed in the density contour plots that is formation of a vorticity ahead of the heat shield and moves toward the stagnation region with the increasing the transonic speeds. The bow shock wave stand-off distance is calculated and compared with the asymptotic relation. A good agreement is found between them.

References

1. Bogdonoff, S., "Some Experimental Studies of the Separation of Supersonic Turbulent Boundary Layers", Heat Transfer and Fluid Mechanics Institute, University of California, Los Angeles, June, 955, pp.1-23.

2. Ericsson, L. E. and Reding, J. P., "Analysis of Flow Separation Effects on the Dynamics of a Large Space Booster", Journal of Spacecraft and Rockets, Vol. 2, 1965, pp.481-490.

3. Ericsson, L. E., "Steady and Unsteady Terminal Shock Aerodynamics on Cone-cylinder Bodies", NASA CR 61560, October, 1967.

4. Rainey, A. G., "Progress on the Launch Vehicle Buffeting Problem", Journal of Spacecraft and Rockets, Vol. 2, 1965, pp. 289-299.

5. Coe, C. F. and Nute J. B., "Steady and Fluctuating Pressures at Transonic Speeds on Hammer Head Launch Vehicles", NASA TM X-778, 1962.

6. Ahmed, S. and Selvarajan, S., "Investigation of Flow on a Hammer Head Nose Configuration at Transonic Speeds", AIAA paper 91-1711, 1991.

7. Deese, J. E., Gielda, T. P., Agarwal, R. K. and Pavish, D.L., "Prediction of Flow Separation of Launch Vehicle Configuration", AIAA paper 91-1727, June 1991.

8. Baldwin, B. S. and Lomax, H., "Thin Layer Approximation and Algebraic Model for Separated Turbulent Flow", AIAA paper 78-257, January, 1978.

9. Purohit, S. C., "A Navier-Stokes Solution for Bulbous Payload Shroud", Journal of Spacecraft and Rockets, Vol. 23, No. 6, 1986, pp. 590-596.

10. Mehta, R. C., "Flowfield Over Bulbous Heat Shield in Transonic and Supersonic Speeds", Journal of Spacecraft and Rockets, Vol.35, No.1, 1998, pp.102-105.

11. Owens, R. V., "Aerodynamic Characteristics of Spherically Blunted Cones at Mach Numbers from 0.5 to 5.0", NASA TN-D 3088, December, 1965.

12. Peyret, R. and Viviand, H., "Computational Methods for Fluids Flow", Springer-Verlag, New York, 1963, pp.109-111.

13. Jameson, A., Schmidt, W. and Turkel, E., "Numerical Solution of Euler Equations by Finite Volume Method Using Runge-Kutta Time-stepping Scheme", AIAA Paper 81-1259, June, 1981.

14. Mehta, R. C., "Wall Pressure Fluctuations Over a Bulbous Heat Shield of a Satellite Launch Vehicle", Acta Mechanica, Vol. 137, 1999, pp.13-31.

15. Mehta, R. C., "Block Structured Finite Element Grid Generation Method", Paper Accepted for publication in the Computational Fluid Dynamics Journal, 2011.

16. Shang, J. S., "Numerical Simulation of Wing-fuselage Interference", AIAA Paper 81-0084, January, 1981.

17. MacCormack, R. W., "Numerical Methods for Compressible Flow", Workshop-cum-Seminar on Computational Fluid Dynamics held at Vikram Sarabhai Space Centre, Trivandrum, India, December 14-21, 1981.

18. Frank, W. and Zierep, J., "Schallnahe Überschallströmung um rotationssymmetrische Körper", Acta Mechanica, Vol. 19, 1974, pp. 277-287.

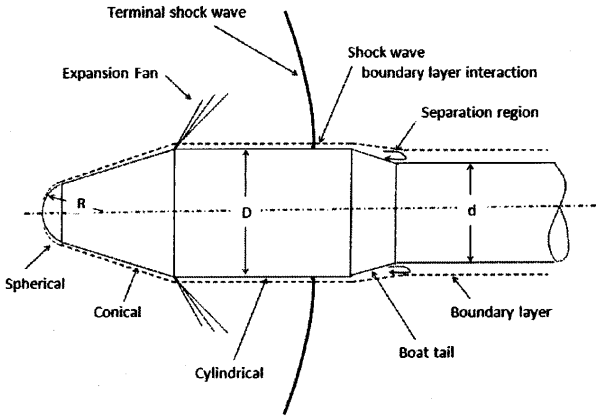

Fig.1a Schematic Sketch for Flowfield Over Payload Fairing at Transonic Mach Number

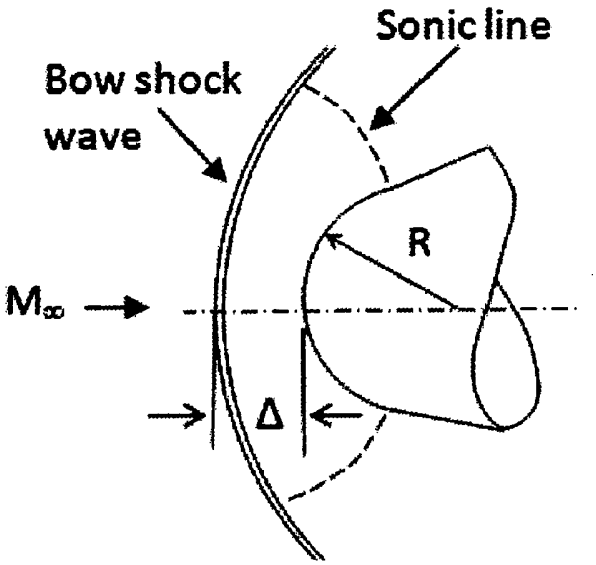

Fig.1b Schematic Sketch for Flowfield Over Payload Fairing at Supersonic Mach Number

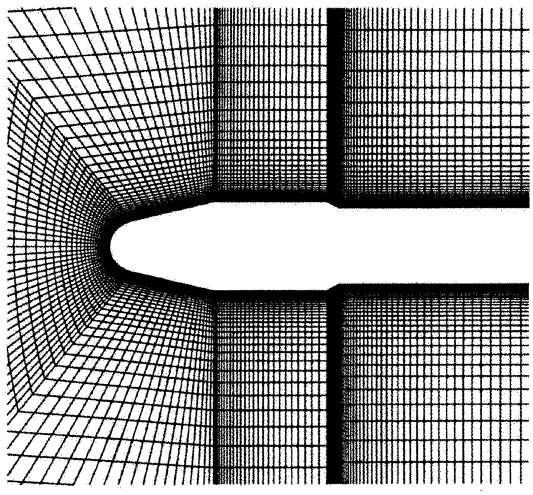

Fig.2 Enlarged View of Grid Arrangement

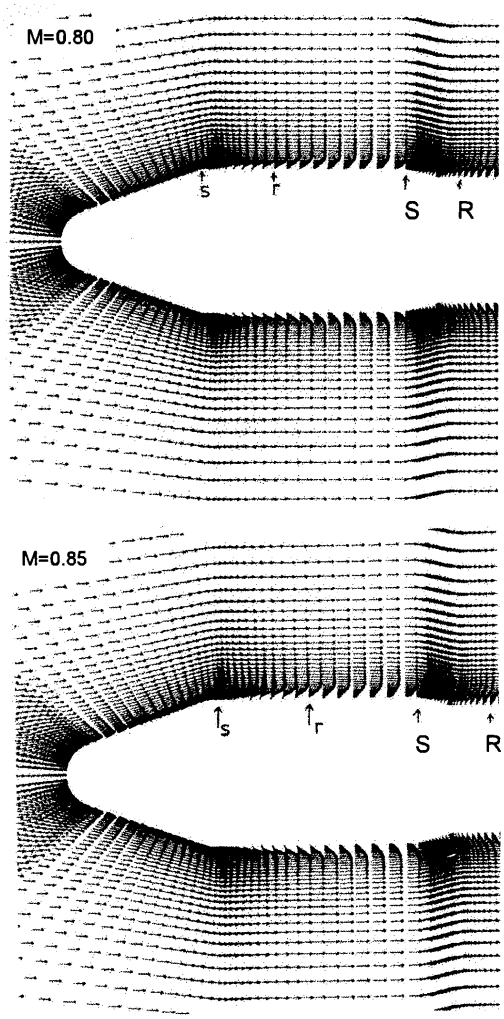

Fig.3 Velocity Vector Plots at Transonic Mach Number

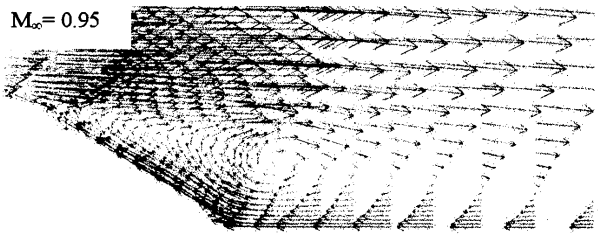

Fig.4 Enlarged View of Separation Region in the Boat-tail Region of Heat Shield

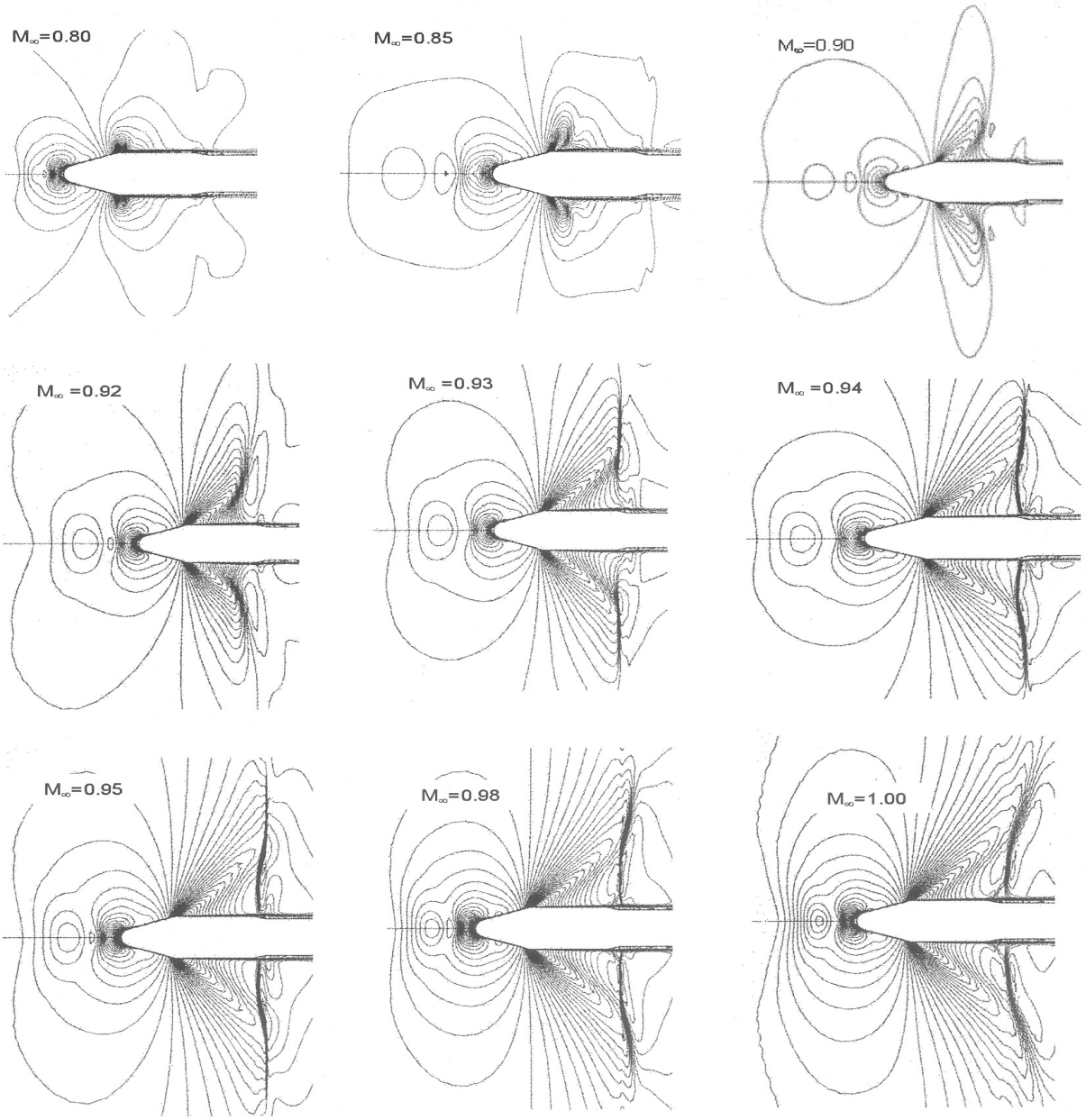

Fig.5 Density Contour Plots at Transonic Mach Number

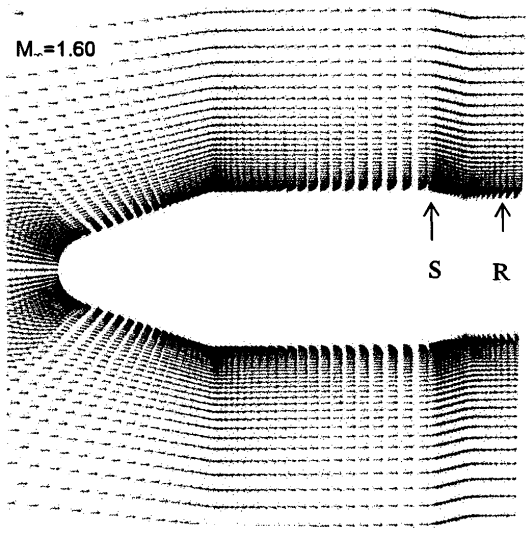

Fig.6 Velocity Vector Plots at Supersonic Speed

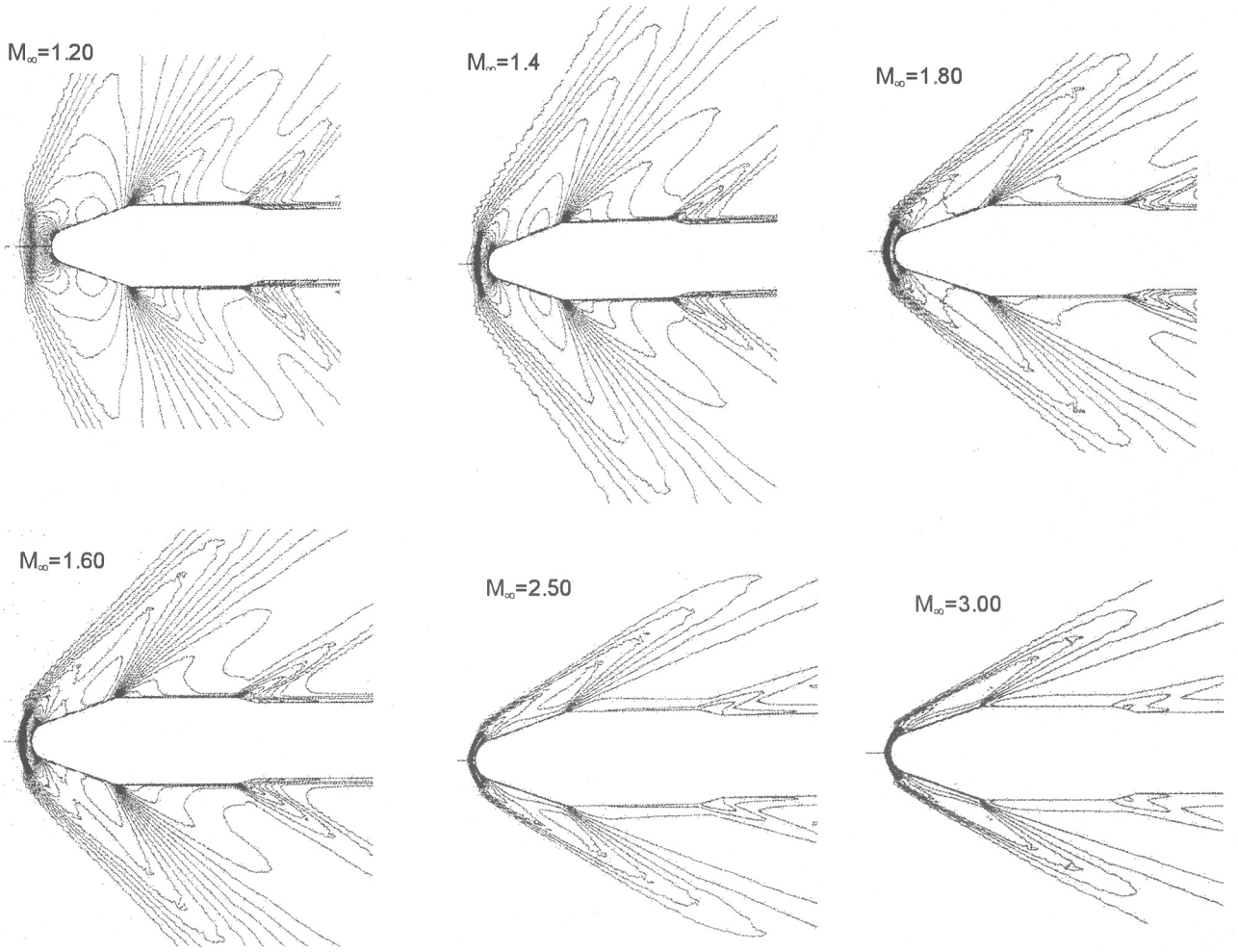

Fig.7 Density Contour Plots at Supersonic Speed

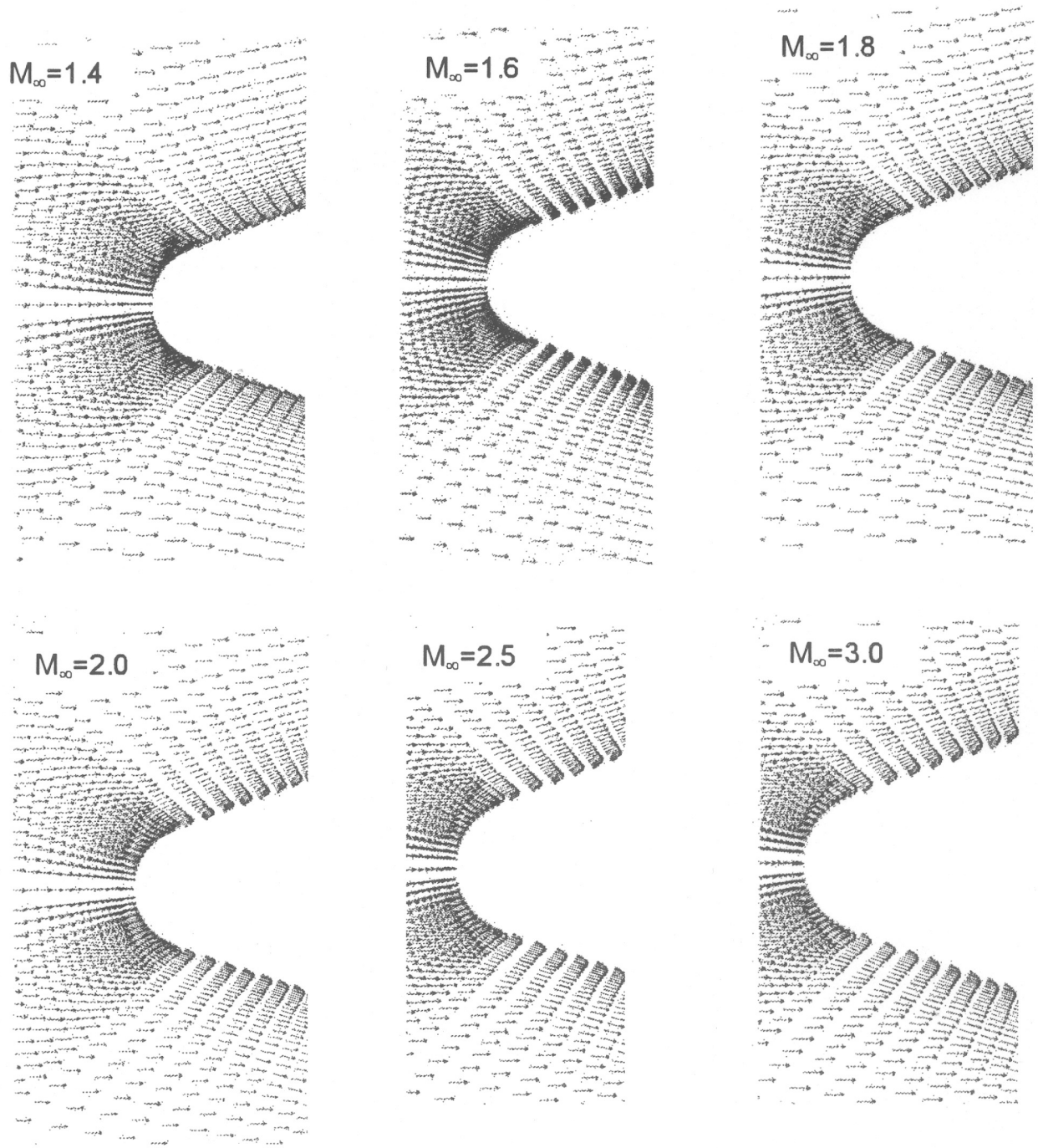

Fig.8 Close-up View of Velocity Vector Plots in the Blunted-cone Region at supersonic Speeds

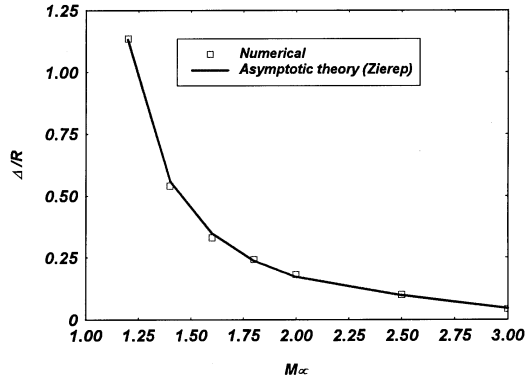

Fig.9 Bow Show Wave Standoff Distance Variation with Freestream Supersonic Speed

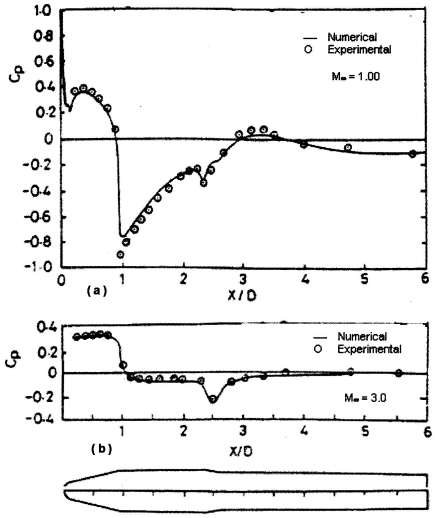

Fig.10 Pressure Coefficient Along the Payload Shroud